# Mechanism for the Homolytic Cleavage of Alkyl Hydroperoxides by the Manganese(III) Dimer $Mn^{III}_2$(2-OHsalpn)$_2$

**M. Tyler Caudle, Pamela Riggs-Gelasco, Andrew K. Gelasco, James E. Penner-Hahn,* and Vincent L. Pecoraro***

Department of Chemistry, University of Michigan, 930 North University Boulevard, Ann Arbor, Michigan 48109-1055

*Received November 14, 1995*[⊗]

The oxidation of $Mn^{III}_2$(2-OHsalpn)$_2$, **1** (2-OHsalpn = 1,3-bis(salicylideneamino)-2-propanol), with *tert*-butyl hydroperoxide was studied in organic media. A one-electron reaction occurs resulting in initial formation of the oxidized $Mn^{III}Mn^{IV}$(2-OHsalpn)$_2$OH species **2** and a *tert*-butoxy radical. The $Mn^{III}Mn^{IV}$(2-OHsalpn)$_2$OH complex can be readily protonated to yield $Mn^{III}Mn^{IV}$(2-OHsalpn)$_2^+$. Upon addition of excess *tert*-butyl hydroperoxide, singlet dioxygen is evolved in an exothermic reaction indicative of radical-induced disproportionation of the hydroperoxide. In the presence of a radical scavenger, the oxygen evolution is strongly attenuated. This system was observed to oxygenate cyclohexene to yield 2-cyclohexen-1-one, 2-cyclohexen-1-ol, and traces of cyclohexene oxide. Cumene is oxygenated to 2-phenyl-2-propanol and acetophenone, and cyclohexane is oxygenated to cyclohexanone and cyclohexanol. However, $^{18}$O-labeling experiments show that the oxygen in the products results exclusively from reactions with aerobic dioxygen and not from the *tert*-butyl hydroperoxide oxidant. These results indicate that oxygenation occurs by radical-initiated aerobic autoxidation and not *via* oxo transfer from a high-valent manganese oxo species. **2** was studied by UV−vis, IR, NMR, EXAFS, XANES, and EPR spectroscopies, which support the assignment of a dinuclear manganese(III/IV) terminal hydroxo structure. **2** was also formed by the direct reaction of $Mn^{III}Mn^{IV}$(2-OHsalpn)$_2^+$ with $OH^-$, further supporting the description of **2** as having a terminal hydroxide ligand. The kinetics of its formation from **1** and *tert*-butyl hydroperoxide were examined and found to be first-order in peroxide. Titration experiments confirm that 1 equiv of peroxide is required to convert **1** to **2**, supporting the conclusion that the peroxide undergoes a one-electron reduction. This system demonstrates that oxy radicals formed from *homolytic* one-electron cleavage of a peroxide by a manganese(III) complex can give small amounts of olefin oxidation species (i.e. epoxides) normally considered evidence for high-valent manganese oxo-transfer chemistry. It therefore underscores the need to test any system for which high-valent metal oxo transfer is proposed to occur using rigorous oxygen-labeling experiments to determine the source of oxygen.

## Introduction

The cleavage of peroxy species by metal complexes and the mechanism of olefin epoxidation and alkane hydroxylation[1−16] by such systems have attracted considerable attention. This is largely due to the relevance of O−O bond cleavage to the proposed mechanism for cytochrome P450, bleomycin, and methane monooxygenase activation by peroxy species. In each of these cases, the lower-valent Fe(II) oxidation state is activated by dioxygen but the aerobically stable Fe(III) state can also be activated by peroxy species such as hydrogen peroxide, alkyl hydroperoxides, and peracids. These reactions have been interpreted in terms of high-valent metal oxo intermediates formed by heterolytic cleavage of the O−O bond, in part by analogy with known manganese systems involving metal oxo intermediates. While high-valent manganese oxo compounds have been isolated[17−19] and analyzed *in situ*,[12−16] analogous high-valent iron oxo species have not been isolated, though evidence exists for the formation of transient high-valent ferryl heme and model heme intermediates[20−26] *in situ*. However, recent reports suggest that, at least for certain model heme[5] and

* Authors to whom correspondence should be addressed.

[⊗] Abstract published in *Advance ACS Abstracts,* May 15, 1996.

(1) Ménage, S.; Wilkinson, E. C.; Que, L.; Fontecave, M. *Angew. Chem., Int. Ed. Engl.* **1995**, *34*, 203−205.
(2) Tétard, D.; Rabion, A.; Verlhac, J.-B.; Guilhem, J. *J. Chem. Soc., Chem. Commun.* **1995**, 531−532.
(3) Arends, I. W. C. E.; Ingold, K. U.; Wayner, D. D. M. *J. Am. Chem. Soc.* **1995**, *117*, 4710−4711.
(4) Rabion, A.; Chen, S.; Wang, J.; Buchanan, R. M.; Seris, J.-L.; Fish, R. *J. Am. Chem. Soc.* **1995**, *117*, 12356−12357.
(5) Grinstaff, M. W.; Hill, M. G.; Birnbaum, E. R.; Schaefer, W. P.; Labinger, J. A.; Gray, H. B. *Inorg. Chem.* **1995**, *34*, 4896−4902.
(6) Weber, L.; Hommel, R.; Behling, J.; Haufe, G.; Hennig, H. *J. Am. Chem. Soc.* **1994**, *116*, 2400−2408.
(7) Buchanan, R. M.; Chen, S.; Richardson, J. F.; Bressan, M.; Forti, L.; Morvillo, A.; Fish, R. H. *Inorg. Chem.* **1994**, *33*, 3208−3209.
(8) Goldstein, A. S.; Beer, R. H.; Drago, R. S. *J. Am. Chem. Soc.* **1994**, *116*, 2424−2429.
(9) Horwitz, C. P.; Creager, S. E.; Murray, R. W. *Inorg. Chem.* **1990**, *29*, 1006−1011.
(10) Jørgensen, K. A. *Chem. Rev.* **1989**, *89*, 431−458.
(11) Koola, J. D.; Kochi, J. K. *J. Org. Chem.* **1987**, *52*, 4545−4553.
(12) Groves, J. T.; Stern, M. K. *J. Am. Chem. Soc.* **1987**, *109*, 3812−3814.
(13) Groves, J. T.; Stern, M. K. *J. Am. Chem. Soc.* **1988**, *110*, 8628−8638.
(14) Rodgers, K. R.; Goff, H. M. *J. Am. Chem. Soc.* **1988**, *110*, 7049−7060.
(15) Balasubramanian, P. N.; Sinha, A.; Bruice, T. C. *J. Am. Chem. Soc.* **1987**, *109*, 1456−1462.
(16) Srinivasan, K.; Michaud, P.; Kochi, J. K. *J. Am. Chem. Soc.* **1986**, *108*, 2309-2320.
(17) MacDonnell, F. M.; Fackler, N. L. P.; Stern, C.; O'Halloran, T. V. *J. Am. Chem. Soc.* **1994**, *116*, 7431−7432.
(18) Collins, T. J.; Gordon-Wylie, S. W. *J. Am. Chem. Soc.* **1989**, *111*, 4511−4513.
(19) Collins, T. J.; Powell, R. D.; Slebodnick, C.; Uffelman, E. S. *J. Am. Chem. Soc.* **1990**, *112*, 899−901.
(20) Ozawa, S.; Watanabe, Y.; Morishima, I. *Inorg. Chem.* **1992**, *31*, 4042−4043.
(21) Mandon, D.; Weiss, R.; Jayaraj, K.; Gold, A.; Terner, J.; Bill, E.; Trautwein, A. X. *Inorg. Chem.* **1992**, *31*, 4404−4409.

S0020-1669(95)01462-5 CCC: $12.00 

nonheme[3,4] iron systems, the organic oxidation data are better explained by a radical mechanism involving homolytic cleavage of the peroxy bond, resulting in formation of an organic oxo radical which initiates subsequent substrate oxidation. Since studies on manganese analogues are often cited as mechanistic models for organic oxidation by iron systems,[2,13−15,27−29] further examination of the mechanism for radical substrate oxidation by non-porphyrin manganese complexes is needed.

We have recently been investigating the mechanism by which the dinuclear alkoxide-bridged manganese(III) complex $Mn^{III}_2$(2-OHsalpn)$_2$, **1** (2-OHsalpn = 1,3-bis(salicylideneamino)-2-propanol), is oxidized by organic peroxides in order to develop

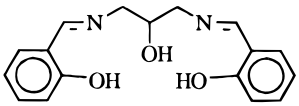

2-OHsalpn

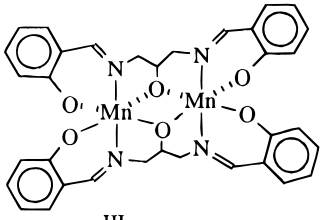

$Mn^{III}_2$(2-OHsalpn)$_2$, **1**

general strategies for chemically accessing higher-valent states of multinuclear Mn clusters. The reactivity of this complex with peroxides is interesting for two reasons. First, **1** has been shown to execute an efficient catalase reaction,[30] disproportionating hydrogen peroxide by cycling between the $Mn^{III}_2$ and $Mn^{II}_2$ oxidation states to yield dioxygen and water, eq 1. This

$$2H_2O_2 \rightarrow O_2 + 2H_2O \qquad (1)$$

reaction involves initial reduction of the $Mn^{III}_2$ dimer to the $Mn^{II}_2$ state by hydrogen peroxide. In contrast, alkyl hydroperoxides oxidize **1** by one electron, to yield a $Mn^{III}Mn^{IV}$ oxidation state. This difference in reactivity between hydrogen peroxide and organic peroxides is significant in that one-electron oxidation of the $Mn^{III}_2$ complex requires homolytic cleavage of the peroxy bond.

Second, crystal structures of $Mn^{III}_2$(2-OHsalpn)$_2$ and $Mn^{III}Mn^{IV}$(2-OHsalpn)$_2^+$ oxidation states have been determined[31] and show that both the III/III and III/IV oxidation states can exist in a free form and a solvated form, Scheme 1 (ring substitution not shown; **3** and **4** correspond to different ring-substituted derivatives). This unique coordinative unsaturation is advantageous in that, in noncoordinating solvents, reactive ligands can insert at the solvation site without dissociating donors from the 2-OHsalpn ligand. Furthermore, the solvated and unsolvated $Mn^{III}_2$(2-OHsalpn)$_2$ and $Mn^{III}Mn^{IV}$(2-OHsalpn)$_2^+$ exhibit very clean spectroscopic characteristics, giving us a very effective set of tools with which to characterize observable intermediates in the reaction of **1** with peroxides. In this paper, we present data showing that the oxidation of **1** by tertiary alkyl hydroperoxides in acetonitrile results in the initial formation of $Mn^{III}Mn^{IV}$(2-OHsalpn)$_2$OH, **2**, and that the structure of **2** is consistent with the solvated $Mn^{III}Mn^{IV}$(3,5-Cl$_2$-OHsalpn)$_2$(THF)$^+$ complex **6** in Scheme 1, where the hydroxide ligand occupies the labile solvation site. We have also observed that this system evolves singlet dioxygen in the absence of any reactive substrate. In the presence of a radical scavenger, the oxygen evolution is attenuated, but aerobic oxidation of activated organics is observed when *tert*-butyl hydroperoxide is added to a solution of **1** and the desired substrate. These data are interpreted in terms of the alkoxy radical generated by the initial one-electron oxidation of **1** by the alkyl hydroperoxide.

**Scheme 1**

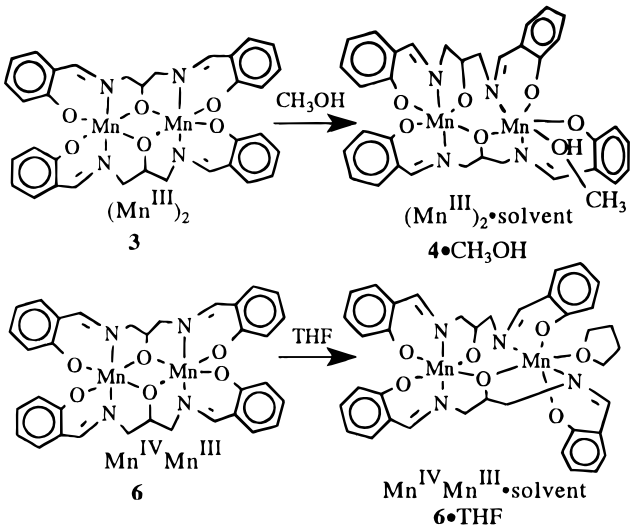


## Experimental Section

**Materials and Equipment.** HPLC grade acetonitrile was treated with anhydrous $CuSO_2$ and CaH, followed by distillation over $P_2O_5$. Other solvents were purchased in HPLC grade and used without further purification. $Mn^{III}_2$(2-OHsalpn)$_2$, **1**, and the ring-substituted derivatives $Mn^{III}_2$(5-Cl-2-OHsalpn)$_2$, **3**, and $Mn^{III}_2$(3,5-Cl$_2$-2-OHsalpn)$_2$, **4**, were prepared according to previous synthetic procedures.[31−33] The oxidized $Mn^{III}Mn^{IV}$ derivatives $Mn^{III}Mn^{IV}$(5-Cl-2-OHsalpn)$_2$ClO$_4$, **5**, and $Mn^{III}Mn^{IV}$(3,5-Cl$_2$-2-OHsalpn)$_2$ClO$_4$, **6**, were prepared by bulk electrolysis of the corresponding $Mn^{III}_2$ compound.[31] *Caution*! Perchlorate salts are potentially shock sensitive and should be handled with appropriate precautions. The solvated complexes $Mn^{III}_2$(3,5,-Cl$_2$-2-OHsalpn)$_2$(CH$_3$OH), **4**·CH$_3$OH, and $Mn^{III}Mn^{IV}$(3,5-Cl$_2$-2-OHsalpn)$_2$(THF)ClO$_4$, **6**·THF, were prepared by recrystallization of **4** from methanol and **6** from tetrahydrohydrofuran. Cyclohexene (Eastman Kodak) and cyclohexane (Sigma/Aldrich) were analyzed by GC to determine that no oxidation products existed at detectable levels. Cumene (Aldrich) was purified by distilling under nitrogen, followed by passage through a column of 200−400 mesh silica gel to remove peroxide impurities. Visible spectra were recorded on a Perkin-Elmer Lambda 9 scanning instrument. Gas chromatograms were recorded using a Hewlett-Packard 5890A gas chromatograph equipped with a medium-bore fused-silica column, FID

(22) Groves, J. T.; Haushalter, R. C.; Nakamura, M.; Nemo, T. E.; Evans, B. J. *J. Am. Chem. Soc.* **1981**, *103*, 2884−2886.
(23) Kean, R. T.; Oertling, W. A.; Babcock, G. T. *J. Am. Chem. Soc.* **1987**, *109*, 2185−2187.
(24) Fujii, H.; Ichikawa, K. *Inorg. Chem.* **1992**, *31*, 1110−1112.
(25) Arasasingham, R. D.; Cornman, C. R.; Balch, A. L. *J. Am. Chem. Soc.* **1989**, *111*, 7800−7805.
(26) Penner-Hahn, J. E.; Eble, K. S.; McMurry, T. J.; Renner, M.; Balch, A. L.; Groves, J. T.; Dawson, J. H.; Hodgson, K. O. *J. Am. Chem. Soc.* **1986**, *108*, 7819−7825.
(27) Creager, S. E.; Raybuck, S. A.; Murray, R. W. *J. Am. Chem. Soc.* **1986**, *108*, 4225−4227.
(28) Sorokin, A.; Robert, A.; Meunier, B. *J. Am. Chem. Soc.* **1993**, *115*, 7293−7299.
(29) Fish, R. H.; Fong, R. H.; Oberhausen, K. J.; Konings, M. S.; Vega, M. C.; Christou, G.; Vincent, J. B.; Buchanan, R. M. *New. J. Chem.* **1992**, *16*, 727−733.
(30) Gelasco, A.; Pecoraro, V. L. *J. Am. Chem. Soc.* **1993**, *115*, 7928−7929.
(31) Gelasco, A.; Pecoraro, V. L. Manuscript in preparation.
(32) Bertoncello, K.; Fallon, G. D.; Murray, K. S.; Tiekink, E. R. T. *Inorg. Chem.* **1991**, *30*, 3562−3568.
(33) Bonadies, J. A.; Kirk, M. L.; Lah, M. S.; Kessissoglou, D. P.; Hatfield, W. E.; Pecoraro, V. L. *Inorg. Chem.* **1989**, *28*, 2037−2044.

detectors, and a Hewlett Packard 3393A integrator. An injector temperature of 200 °C, an initial column temperature of 30 °C, and a temperature ramp of 20 °C/min were used. GC/MS were recorded on a Finnegan Model 4000 GC/MS system with GC parameters set the same as above. $^1$H NMR spectra in the paramagnetically shifted region were recorded at room temperature using a Bruker AC-200 FTNMR spectrometer with an acquisition time of 0.10 s. The 77 K EPR spectra were run on a Bruker ER 200E instrument at 20 mW with the sample tube immersed in a liquid $N_2$-filled finger Dewar flask placed between the magnets. The low-temperature spectra were run on the Bruker ER 200E with an Air Products OC-20 helium cryostat and an Oxford 3120 temperature controller. A PC interface was used for data collection. UV−visible kinetic studies were performed at 25 °C on an OLIS RSM-1000 rapid-scanning stopped-flow device.

**Purification of *tert*-Butyl Hydroperoxide.** Reagent grade *tert*-butyl hydroperoxide (Aldrich 5.0−6.0 M solution in decane) was dissolved in diethyl ether and extracted into cold 15% sodium hydroxide. The aqueous layer was isolated and carefully acidified with concentrated HCl while being chilled. The resulting aqueous solution was then extracted with diethyl ether. The organic phase was dried with magnesium sulfate and the solvent removed by rotary evaporation under hard vacuum while the evaporation flask was cooled in an ice bath. This gave a viscous clear liquid that analyzed as >98% pure *tert*-butyl hydroperoxide by GC and iodometric titration (10.1 mequiv/g). (*Caution*! Neat organic peroxides are an explosion hazard. They should be stored cold, in small quanitites, and they should be handled behind a blast shield.)

**Preparation of $Mn^{III}Mn^{IV}$(2-OHsalpn)$_2$OH (2).** In a typical preparation, 1.0 g of $Mn^{III}_2$(2-OHsalpn)$_2$·acetone was dissolved in 100 mL of butyronitrile with gentle warming, and the solution was cooled to 5 °C. 1 equiv of *tert*-butyl hydroperoxide was added with vigorous stirring, resulting in a color change from dark green to dark brown. After 1−2 min, the cold solution was poured into 600 mL of chilled hexane to give a cloudy brown solution. The solution was immediately filtered to give a brown powder, which was air-dried for 10 min and immediately stored below −20 °C. This gave a 75% yield of $Mn^{III}$-$Mn^{IV}$(2-OHsalpn)$_2$OH·$x$H$_2$O ($x$ = 1−2). Anal. found (calcd) for $x$ = 1.5: $Mn^{III}Mn^{IV}$ C, 55.8 (56.0); H, 4.7 (4.5); N, 7.9 (7.7); Mn, 15.5 (15.1).

**Preparation of $Mn^{III}Mn^{IV}$(2-OHsalpn)$_2^+$ (7).** In a typical preparation, 1.0 g of $Mn^{III}_2$(2-OHsalpn)$_2$·acetone was dissolved in 50 mL of dichloromethane. A second solution containing 1 equiv of *tert*-butyl hydroperoxide and 2 equiv of triethylamine hydrochloride in 10 mL of dichloromethane was added with stirring. Almost immediately, a brown precipitate formed. This was collected and recrystallized from acetonitrile to give $Mn^{III}Mn^{IV}$(2-OHsalpn)$_2^+$Cl$^-$·CH$_3$CN in 65% yield. Anal. Found (calc): C, 55.4 (55.7); H, 4.5 (4.3); N, 9.0 (9.0); Mn, 13.9 (14.1).

The hexafluorophosphate salt was prepared by ion exchange of $Mn^{III}$-$Mn^{IV}$(2-OHsalpn)$^{2+}$Cl$^-$ with potassium hexafluorophosphate in methanol. The initial precipitate of KCl was removed and the solvent evaporated. The resulting solid residue was washed with water to remove any remaining $KPF_6$ and was recrystallized from acetone to give $Mn^{III}Mn^{IV}$(2-OHsalpn)$_2^+$PF$_6^-$·C$_3$H$_6$O(H$_2$O)$_2$ in 70% yield. Anal. Found (calc): C, 47.3 (47.3); H, 4.2 (4.3); N, 6.0 (6.0); Mn, 12.2 (11.7).

**X-ray Absorption Analysis of $Mn_2$(2-OHsalpn)$_2$OH (2).** Solid samples of **2** were frozen in liquid nitrogen until just prior to dilution in boron nitride in approximately a 1:1 (v:v) ratio (sample preparation time = 10 min). Data were collected in transmission mode using $N_2$-filled ion chambers at beamlines 2−3 and 7−3 at Stanford Synchrotron Radiation Laboratory using a Si(220) double-crystal monochromator. Harmonic rejection was achieved by detuning the incident intensity by 50%. Spectra were calibrated by simultaneously measuring the absorption spectrum of $KMnO_4$; the distinctive $KMnO_4$ pre-edge feature was assigned a value of 6543.3 eV. Reported spectra are the average of two 45-min scans (0.05 Å$^{-1}$ spacing, $k^3$-weighted collection time). Sample temperature was maintained at 10 K with an Oxford continuous-flow liquid helium cryostat.

A fitted line was extrapolated through the pre-edge region (6300−6535 eV) and subtracted from the data prior to calculation and subtraction of a cubic 3 region spline to yield the EXAFS oscillations. The $k^3$-weighted EXAFS data were used for all analyses to offset the decrease in EXAFS amplitude at high $k$. Data were analyzed over a $k$ range of 1.5−11.5 Å$^{-1}$. Phase and amplitude functions were calculated using the program FEFF3.0, which utilizes single-scattering curved-wave formalism.[34,35] $R$ and $\sigma$ were varied in a nonlinear least-squares-fitting algorithm. The coordination number was held fixed, but all reasonable values were utilized in fits and compared. In studies on crystallographically characterized model complexes,[36] the optimum values for $\Delta E_0$ and the scale factor were determined to be 10 eV and 0.9, respectively, and were held fixed. Fit quality was judged by using the mean-square deviation, $F$. The quantity $F'$ was calculated to correct the improvement in fit for changes in the number of variable parameters (see definitions in Table S2, Supporting Information). Calculated fits used data filtered over a single wide range to eliminate high-frequency noise.

Normalized edge spectra were obtained by fitting a single polynomial through the entire range of the spectrum. The coefficients of this polynomial were refined in a least-squares sense to optimize the data above and below the edge to the calculated McMaster values of X-ray absorption cross sections.[37,38] The observed XANES spectra were fit using a linear combination of spectra drawn from a library of authentic Mn(II), Mn(III), and Mn(IV) model compounds, refining in a least squares sense the coefficients of the linear combination (i.e. the fractional contribution of each model spectrum to the unknown spectrum).

**Singlet Oxygen Detection.** Singlet oxygen evolution was detected by monitoring the emission intensity at 1270 nm upon addition of *tert*-butyl hydroperoxide to a saturated solution of **1** in methylene chloride. This emission was compared to the emission intensity observed upon addition of 1 $\mu$mol of hydrogen peroxide to an aqueous solution of Clorox. The solution, in a standard spectrophotometer cell, was imaged onto a liquid $N_2$-cooled Ge detector (North Coast) through a 1270 nm interference filter. In order to improve the signal to noise ratio so that the emission could be detected, a rotating-sector light chopper was placed between the sample and the detector and the output of the detector processed by a two-phase lock-in amplifier in resultant mode (Ithaco). The best signals were obtained at a chopping frequency of ca. 15−40 Hz.

**Kinetic Experiments.** Stock solutions of *tert*-butyl hydroperoxide for these experiments were standardized iodometrically against sodium thiosulfate. The reaction of **1** with *tert*-butyl hydroperoxide was monitored under pseudo-first-order conditions of excess peroxide by rapidly mixing equal volumes of **1** and peroxide solutions in acetonitrile at room temperature using the stopped-flow apparatus and monitoring the time-dependent spectrum with the rapid-scanning monochromator. Absorbance data over the range from 320 to 650 nm (resolution ≈ 2 nm) were globally fit to a first-order exponential decay to give the experimental pseudo-first-order rate constant, $k_{obs}$.

**Organic Oxidation Experiments.** In a typical experiment, 6.8 mg (8.9 $\mu$mol) of **1**·acetone and 2.0 mL of the desired organic substrate were dissolved in 50 mL of $CH_3CN$. This solution was placed in a 100 mL round-bottom flask attached to a gas-tight gas buret apparatus, degassed, and pressurized to 1 atm with dioxygen. No organic oxidation was observed under these conditions. Then 0.050 g of *tert*-butyl hydroperoxide was injected and aliquots were removed by syringe at intervals for GC analysis. The decrease in oxygen head pressure in the system was monitored with time as well. This experiment was repeated using $^{18}O_2$ as the head gas, and incorporation of $^{18}$O was determined by GC/MS.

## Results

The one-electron oxidation of **1** using *tert*-butyl hydroperoxide in acetonitrile or methylene chloride proceeds cleanly in

(34) Rehr, J. J.; de Leon, J. M.; Zabinsky, S. I.; Albers, R. C. *J. Am. Chem. Soc.* **1991**, *113*, 5135−5140.
(35) Rehr, J. J.; Albers, R. C. *Phys. Rev.* **1990**, *B41*, 8139.
(36) Riggs-Gelasco, P. Ph.D. Thesis, University of Michigan, 1994.
(37) Waldo, G. S. Ph.D. Thesis, University of Michigan, 1991.
(38) McMaster, W. H.; Grande, K. D.; Millet, J. H.; Hubbel, J. H. *Compilation of X-ray Cross Sections*; National Technical Information Services: Springfield, VA, 1969; Vol. UCRL-50174.
(39) Larson, E.; Haddy, A.; Kirk, M. L.; Sands, R. H.; Hatfield, W. E.; Pecoraro, V. L. *J. Am. Chem. Soc.* **1992**, *114*, 6263−6265.

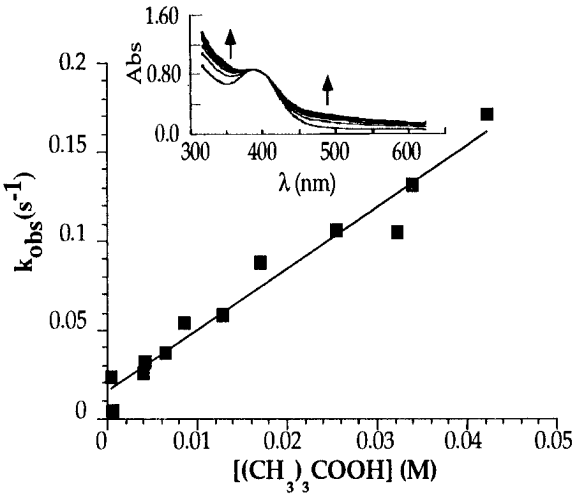


**Figure 1.** Kinetics of the oxidation of $Mn^{III}_2$(2-OHsalpn)$_2$ (**1**) by *tert*-butyl hydroperoxide in acetonitrile. [**1**] = 0.050 mM. [ROOH] = 0.42−42 mM. $T$ = 25 °C. Inset. Time-dependent spectrum upon oxidation of **1** by *tert*-butyl hydroperoxide. [**1**] = 0.073 mM. [ROOH] = 6.445 mM. $T$ = 25 °C. Arrows show spectroscopic change upon addition of ROOH.

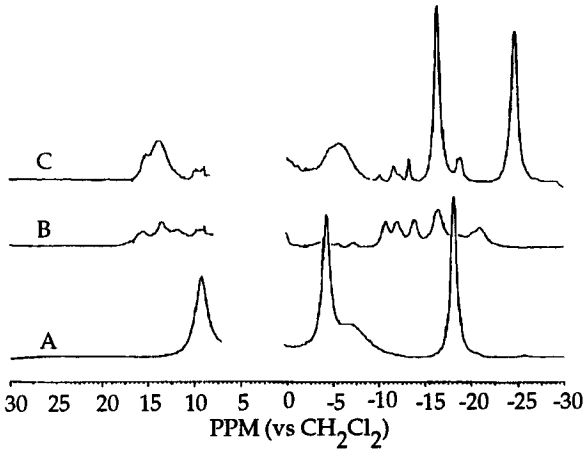


**Figure 2.** Oxidation of $Mn^{III}_2$(2-OHsalpn) $_2$ (**1**) by *tert*-butyl hydroperoxide followed by $^1$H NMR in the paramagnetic region: (A) **1;** (B) 1 equiv of *tert*-butyl hydroperoxide added to solution in (A); (C) 1 equiv of 2,6-lutidinium hexafluorophosphate added to solution in (B). [**1**] = 0.010 M. Solvent = $CD_2Cl_2$. $T$ = 25 °C. Intensity was scaled to the residual solvent peak.

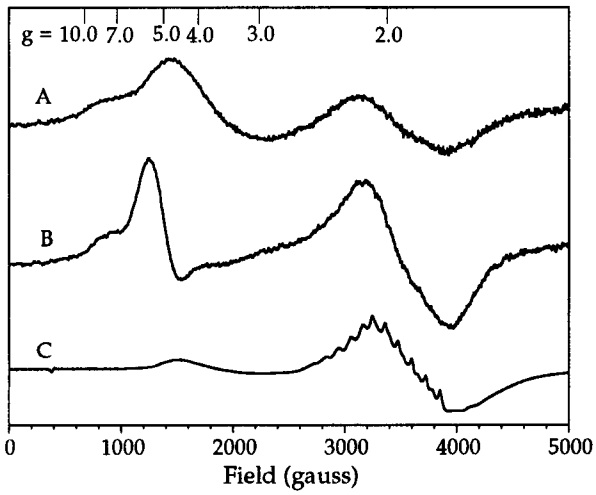


**Figure 3.** Oxidation of $Mn^{III}_2$(2-OHsalpn)$_2$ (**1**) by *tert*-butyl hydroperoxide followed by EPR spectroscopy: (A) 1 equiv of *tert*-butyl hydroperoxide added to **1**; (B) 1 equiv of 2,6-lutidinium hexafluorophosphate added to the solution in (A); (C) 1 equiv of *tert*-butyl hydroperoxide added to **1**, spectrum measured at 20 K. [**1**] = 0.010 M. Solvent = butyronitrile. $T$ = 77 K.

the presence of 1 equiv of weak acid to give the $Mn^{III}Mn^{IV}$(2-OHsalpn)$_2^+$ cation, **7**. However, in the absence of a proton source, the intermediate species **2** is formed. The time-dependent formation of **2** in acetonitrile was followed in the stopped-flow time regime using visible spectroscopy, Figure 1, inset. These data show a spectroscopic shift from the $Mn^{III}_2$ complex having a distinct $\lambda_{max}$ at 395 nm to the $Mn^{III}Mn^{IV}$ hydroxide complex, **2**, having only a shoulder in the visible region at ≈400 nm. Addition of a trialkylammonium salt results in a second fast spectroscopic shift to give the ill-defined shoulder characteristic of the unligated $Mn^{III}Mn^{IV}$ species, **7**. The kinetics of the formation reaction were measured as a function of *tert*-butyl hydroperoxide concentration under conditions of excess peroxide, and the pseudo-first-order rate constant, $k_{obs}$, was found to be linearly dependent on the peroxide concentration, Figure 1, confirming that the rate-limiting step is first-order in peroxide. The slope in Figure 1 gives a second-order rate constant of 3.4 $M^{-1}$ $s^{-1}$. Incremental addition of *tert*-butyl hydroperoxide from 0.0 to 3.0 equiv gives no change in the visible spectrum after 1.0 equiv, Figure S1, which shows that only 1 equiv of peroxide is required to completely oxidize **1**.

The reaction was also followed by $^1$H NMR in the paramagnetically shifted region from +50 to −50 ppm. The paramagnetic $^1$H NMR of **1** in $CD_2Cl_2$ is shown in Figure 2A. Addition of 1 equiv *tert*-butyl hydroperoxide results in the loss of the major signals at 9.0, −4.0, −6.5, and −17.5 ppm and the appearance of the complex and less intense spectrum in Figure 2B. Scanning the paramagnetic region in the peroxide-treated sample from +200 to −200 ppm showed no additional paramagnetically shifted protons with the applied NMR parameters. Addition of a slight excess of 2,6-lutidinium hexafluorophosphate to the same sample results in the appearance of new signals at 13.5, −6.0, −16.0, and −25 ppm, identical to those of the unsolvated $Mn^{III}Mn^{IV}$ complex **7** dissolved in $CD_2Cl_2$. Dissolution of solid **2** into $CD_2Cl_2$ resulted in a weak paramagnetic spectrum as in Figure 2B. Addition of excess lutidinium hexafluorophosphate to this solution resulted in the appearance of a spectrum identical to Figure 2C.

The changes in oxidation state and electronic structure were monitored using EPR spectroscopy. In frozen glassy butyronitrile at 77 K, **1** exhibits no EPR signal in the range $g$ = 10−2. Addition of 1 equiv of *tert*-butyl hydroperoxide results in a 77 K EPR spectrum with broad features at $g$ = 1.9 and $g$ = 4.7, Figure 3A, characteristic of Mn(IV) complexes with strong oxygen donors. Addition of 2,6-lutidinium hexafluorophosphate causes the $g$ = 4.7 signal to shift to $g$ = 5.3, while leaving the high-field signal invariant at $g$ = 1.9, Figure 3B. The low-field shoulder at $g$ = 7.5 does not move upon addition of acid. The $g$ values of 1.9 and 5.3 are consistent with $g$ values previously determined for $Mn^{III}Mn^{IV}$(2-OHsalpn)$_2^+$ in DMF.[39] The features at $g$ = 7.5, 4.7, and 1.9 are evident in the EPR spectrum upon the addition of stoichiometric tetrabutylammonium hydroxide to **7**. Upon cooling of **2** to 20 K, a pattern of at least 12 hyperfine lines becomes superimposed on the $g$ = 1.9 signal and the signal at $g$ = 4.7 is very attenuated, Figure 3C, consistent with **2** being a dinuclear $Mn^{III}Mn^{IV}$ complex with weak spin coupling between the manganese centers.

By precipitation with hexane immediately after oxidation, a solid was isolated and found by elemental analysis to be consistent with $Mn^{III}Mn^{IV}$(2-OHsalpn)$_2$OH·x$H_2O$, **2**. The infrared spectrum of this solid was measured as an evaporated film (solvent = acetone) and found to be essentially identical

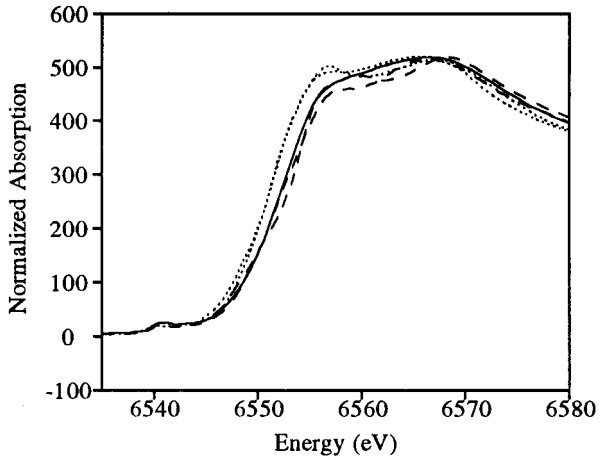


**Figure 4.** Normalized XANES spectra of **2** and model derivatives: dotted lines, $Mn^{III}_2$ derivatives **3** and **4**·$CH_3OH$; dashed lines, $Mn^{III}$-$Mn^{IV}$ derivatives **6** and **6**·THF; solid line, **2**. Conditions were as given in the Experimental Section. Data on **3**, **4**·$CH_3OH$, **6**, and **6**·THF were taken from ref 36.

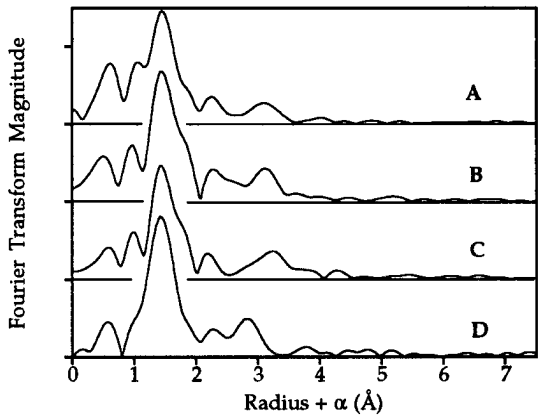


**Figure 5.** Fourier transform of the EXAFS spectra of **2** and model derivatives: FT's were calculated using $k^3$-weighted data over $k$ = 2−11.8 $Å^{-1}$ and are offset vertically for clarity. Conditions were as given in the Experimental Section. (A) **2**; (B) **6**·THF; (C) **4**·$CH_3OH$; (D) **6**. Data for **6**·THF, **4**·$CH_3OH$, and **6** were taken from ref 36.

to that for **7**, suggesting considerable structural similarity between the two complexes. It has not yet proven possible to obtain X-ray quality crystals of **2**. Therefore, X-ray absorption measurements were made on samples of powdered **2**, as well as on the related model derivatives **4**·$CH_3OH$, **6**·THF, **3**, and **6**, shown in Scheme 1. These particular model compounds were chosen for comparison since they have all been crystallographically characterized[31] and represent all four structure types for this motif.

The XANES spectrum for **2** is very similar to those for the other $Mn^{III}Mn^{IV}$ complexes, **6**·THF and **6**, but it is distinct from those for the $Mn^{III}_2$ complexes **4**·$CH_3OH$ and **3** as shown in Figure 4. This is consistent with the general trend for edge energies of manganese dimers to increase as the oxidation state increases.[40] The edge energy of **2** is essentially identical to that for the characterized $Mn^{III}Mn^{IV}$ complexes, providing further evidence that the intermediate hydroxo species **2** exists in the $Mn^{III}Mn^{IV}$ oxidation state. Edge-fitting analyses for the complexes,[36] Table S1 (Supporting Information), are consistent with this oxidation state assignment.

The Fourier transform of the EXAFS region for **2** is compared to those of **4**·$CH_3OH$, **6**·THF, and **6** in Figure 5 and provides further structural insight into **2**. Both **2** and the two solvated dimers, **4**·$CH_3OH$ and **6**·THF, have a defined feature at ($R$ + α) ∼3.3 Å in the FT, Figure 5A−C. This feature is not apparent in the FT of the unsolvated dimer **6**, Figure 5D. The results of the EXAFS curve fitting are given in Table S2 (Supporting Information) for compounds **2** and **6**·THF. In both cases, the EXAFS data require **4** shells of scatterers: Mn−O at 1.9 Å, Mn−N at 2.3 Å, Mn−C at 2.9 Å, and a fourth shell at either 3.3 or 3.7 Å. The first two shells are attributable to Mn−nearest neighbor interactions, with the longer shell reflecting the axial elongation of the Mn(III) ion. The Mn−C shell at 2.9 Å is assigned to Mn−C next nearest neighbor on the basis of comparison with the crystal structure for **6**·THF. The fourth shell can be modeled as a Mn−Mn interaction at 3.3 or 3.7 Å or as a Mn−C interaction at 3.7 Å, with the longer shell distance being superior. We attribute the 3.7 Å shell to a Mn−Mn interaction on the basis of the crystal structure for **6**·THF.[31] The inability to distinguish unambiguously between Mn and C scatterers at this distance is typical of weak single-atom bridged metal-metal interactions.[41] In contrast, the EXAFS data for **6** show unambiguous evidence for a Mn−Mn shell at 3.3 Å, consistent with the crystallographic Mn−Mn distance in **6**.[31]

The reaction of **1** with *tert*-butyl hydroperoxide was probed by a variety of methods designed to determine whether a radical species is released. In the simplest experiment, a large excess of *tert*-butyl hydroperoxide was reacted with **1** in $CH_2Cl_2$ or $CH_3CN$. After a short lag time, a vigorous and exothermic evolution of gas was observed. The gas was determined to be dioxygen using a Clark-type oxygen-sensitive electrode. Spectroscopic emission studies revealed intensity at 1268 nm, characteristic of dioxygen produced in the singlet state via peroxy radical recombination.[42−44] The organic products, observed by GC analysis of the reaction mixture, consist of *tert*-butyl alcohol with traces of di-*tert*-butyl peroxide. If cumyl hydroperoxide is used in place of *tert*-butyl hydroperoxide, 2-phenyl-2-propanol and acetophenone are formed, consistent with the decomposition of cumyl peroxyl radicals. Freezing a reaction mixture during dioxygen evolution and measuring its EPR spectrum reveals an intense, sharp radical singlet at $g$ = 2, suggestive of the formation of alkoxy or alkylperoxy radicals. Addition of an excess of a radical-scavenging species such as nitrosylbenzene traps the initial radical, as shown by EPR, and severely inhibits oxygen evolution as shown by manometry.

When **1** is reacted with *tert*-butyl hydroperoxide in the presence of cyclohexene, the primary organic products are 2-cyclohexen-1-one (64%) and 2-cyclohexen-1-ol (24%), 2-cyclohexen-1-one oxide (8%), cyclohexene oxide (2%), and bicyclohexene (2%), Figure S2 (Supporting Information). Essentially quantitative oxygen uptake was observed manometrically. When the reaction was performed under anaerobic conditions, the only organic product was bicyclohexene. When the oxidation was performed in an atmosphere of $^{18}O_2$, all of the cyclohexene oxidation products showed incorporation of $^{18}O$ exclusively. Furthermore, the amount of oxidized cyclohexene products continued to increase even after all of the **1** had been converted into the inactive **2**. The oxidation of cumene results in the formation of 2-phenyl-2-propanol and acetophenone, Figure S3 (Supporting Information), the same products observed

(40) Riggs, P. J.; Mei, R.; Yocum, C. F.; Penner-Hahn, J. E. *J. Am. Chem. Soc.* **1992**, *114*, 10650−10651.

(41) Riggs-Gelasco, P. J.; Stemmler, T.; Penner-Hahn, J. E. *Coord. Chem. Rev.* **1995**, *144*, 245−286.

(42) Mendenhall, G. D.; Niu, Q. J. *J. Am. Chem. Soc.* **1992**, *114*, 165−172.

(43) Sugimoto, H.; Sawyer, D. T. *J. Am. Chem. Soc.* **1988**, *110*, 8707−8708.

(44) Kanofsky, J. R. *J. Org. Chem.* **1986**, *51*, 3386−3388.

**Scheme 2**

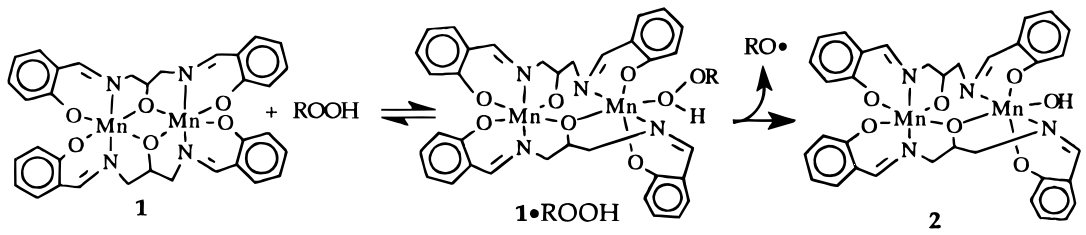


in the decomposition of cumene hydroperoxide by **1**. Oxidation of cyclohexane gives cyclohexanone and cyclohexanol, Figure S4 (Supporting Information).

## Discussion

**Structure of 2.** In the absence of crystallographic data, the most compelling evidence for the structure of **2** comes from the comparison of its EXAFS spectrum with that of previously characterized model compounds. It is clear from the fits to the EXAFS data that **2** is not structurally analogous to the unsolvated compound **6**. The spectrum for **6** is best fit with a Mn−Mn interaction at 3.3 Å, which is consistent with the crystallographically determined Mn−Mn distance in this compound.[31] **2** is more analogous to the solvated complexes **4**·$CH_3$-OH and **6**·THF, which are not fit well with this shorter Mn−Mn distance. The comparison of the EXAFS fitting parameters for analysis of **2** and **6**·THF are shown in Table S2. The best fit parameters assuming a scatterer, either Mn or C, at approximately 3.7 Å are similar for **2** and **6**·THF. However, this scatterer is 0.04 Å longer in **2**. If this is indeed due to Mn scattering, then it is consistent with the manganese bearing the hydroxide being pulled slighty out of the O−N−O−N plane towards the stronger hydroxide ligand. This would result in a slight lengthening of the Mn−alkoxide bond in the bridge and an overall slight elongation of the Mn−Mn distance. This analysis is based on the assumption of a valence-trapped structure for **2**, in which the $Mn^{III}$ ion bears the terminal hydroxo ligand. Valence trapping is observed in the crystal structure of **6**·THF,[31] but it is not clear how replacement of the terminal THF with a hydroxide will affect such valence trapping. It should be expected that the $Mn^{IV}$ center would prefer the nonbridging alkoxide to the terminal hydroxide, enforcing a valence trapping analogous to that observed for **6**·THF, where the $Mn^{III}$ bears the solvating THF. Also, one might expect that in this relatively unhindered system, a structure bearing a terminal hydroxide on a $Mn^{IV}$ should condense with a second ion to form a $\mu$-oxo bridge. We have no indication that $\mu$-oxo formation occurs in this system on a short time scale, and such a formulation for **2** is made unlikely by the observed EPR results. Therefore, the EXAFS data are consistent with the valence-trapped terminal hydroxide structure for **2** as illustrated in Scheme 2.

The paramagnetic $^1$H NMR data in Figure 2 are of limited value in assessing the structural characteristics of **2**. However, it is clear from the NMR data that a fundamental change has been effected upon oxidation by *tert*-butyl hydroperoxide. Figure 2A shows four distinct peaks assigned to complex **1**. Addition of 1 equiv of *tert*-butyl hydroperoxide to **1** gives a new complex with the spectrum in Figure 2B, proposed to be that of **2**. The more complicated spectrum in Figure 2B is consistent with a complex of lower symmetry than that of **1**, which has an inversion center making all of the phenolate rings equivalent. The proposed structure for **2** has no inversion center and will then possess four nonequivalent phenolate rings. This should result in the appearance of additional phenolate NMR signals for **2**, consistent with Figure 2B. The spectrum in Figure 2C, that collected after addition of 1 equiv of lutidinium hexafluorophosphate, shows four predominant peaks with chemical shifts identical to those measured for an independently isolated and characterized sample of the $Mn^{III}Mn^{IV}$(2-OHsalpn)$_2^+$-$PF_6^-$, **7**. The fact that only four signals are observed for **7** suggests that, even though it is in a mixed-valent state, the two equivalent oxidation states ($Mn^{III}$−$Mn^{IV}$ and $Mn^{IV}$−$Mn^{III}$) are in rapid exchange so that the phenolate protons are effectively averaged on the NMR time scale. **7** is not a valence-delocalized complex since the crystal structure is clearly asymmetric, showing two very different Mn coordination environments.[39] This explains why the NMR spectrum of **2**, Figure 2B, is more complicated than that for **7** since placement of a hydroxide on the cluster will tend to "freeze out" the valence-trapped complex so that the phenolate protons are no longer equivalent on the NMR time scale. The NMR data are, therefore, consistent with the reaction of $Mn^{III}_2$(2-OHsalpn)$_2$ with *tert*-butyl hydroperoxide to give $Mn^{III}Mn^{IV}$(2-OHsalpn)$_2$OH, which can then be protonated to yield $Mn^{III}Mn^{IV}$(2-OHsalpn)$_2^+$.

The 77 K EPR and XANES spectra show definitively that one manganese in the dimer **2** has been oxidized. An identical EPR spectrum can be generated by careful addition of 1 equiv of hydroxide to a solution of **7**, which is strong evidence that **2** contains a bound hydroxide ligand. Furthermore, the 20 K EPR spectrum shows 12 hyperfine lines superimposed on the $g = 1.9$ signal, a feature also observed in the low-temperature EPR of **7** in dimethylformamide. These low-temperature multiline signals confirm that more than one manganese contributes to the hyperfine coupling in both **2** and **7**. The temperature-dependent EPR of **7** has been explained on the basis of a temperature-dependent interconversion between an $S = {}^1/_2$ ground state and an $S = {}^3/_2$ low-lying excited state,[39] giving rise to the low-temperature $g = 1.9$ and higher temperature $g = 5.3$ signals, respectively. The temperature dependence of the $g = 1.9$ and 4.7 signals of **2** can be explained by a similar temperature-dependent spin change. However, the $g = 4.7$ signal is shifted upfield for **2** relative to **7**, as might be expected from the stronger hydroxide ligand.

The proposed structure of **2** is significant in that few structurally characterized higher-valent manganese complexes are known having terminal hydroxo ligands[45,46] due to the propensity for such complexes to condense to $\mu$-oxo or $\mu$-hydroxo cores. However, the probable significance of a terminal hydroxo or oxo ligand in water oxidation was recently elucidated using $H_2{}^{18}O$-labeling studies to determine that, in the $S_3$ Kok state of the photosynthetic oxygen-evolving complex (OEC), there are two water molecules which exchange with different rates.[47] The slow-exchanging water is proposed to be coordinated directly to a manganese as a terminal oxo or

(45) (a) Pal, S.; Chan, M. K.; Armstrong, W. H. *J. Am. Chem. Soc.* **1992**, *114*, 6398−6406. (b) Pal, S.; Armstrong, W. H. *Inorg. Chem.* **1992**, *31*, 5417−5423.

(46) Corbella, M.; Costa, R.; Ribas, J.; Fries, P. H.; Latour, J.-M.; Öhrström, L.; Solans, X.; Rodríguez, V. *Inorg. Chem.* **1996**, *35*, 1857−1865.

hydroxo ligand which is oxidized to the level of dioxygen in a still poorly understood cycle. The only model manganese complex to have been shown to oxidize water to dioxygen, a linked bis(manganese porphyrin), also appears to involve a coordinated hydroxo- or oxo-bound intermediate. Therefore, the structure and reactivity of **2**, a non-porphyrin dinuclear manganese complex with a terminal hydroxide, may be very relevant to the mechanism of biological water oxidation, as it is currently envisioned.

**Oxidation of 1 by Homolytic Cleavage of the Peroxy Bond.** The oxidation of **1** by *tert*-butyl hydroperoxide is proposed to occur according to Scheme 2, on the basis of kinetic data and spectroscopy. The proposed pre-equilibrium intermediate, **1**·ROOH, is not observed experimentally but is reasonable in light of the known solvent-dependent equilibrium implied by Scheme 1 and is consistent with the fact that *tert*-butyl hydroperoxide reacts only very slowly with **1** in the presence of methanol, a donating solvent that can compete with the peroxide for the solvent accessible site. The most pertinent aspect of this reaction is the second step in Scheme 2, the one-electron homolytic cleavage of the peroxide to give an alkoxy radical. *tert*-Butyl hydroperoxide has a polarographic half-wave reduction potential at about −0.30 V *vs* SCE in aqueous solution.[48] However, this value is very solvent dependent, and in less polar solvents such as 1:1 methanol/benzene, the half-wave potential is nearly −1.0 V.[49] Complex **1** has a reversible one-electron redox couple ($Mn^{III}_2$ to $Mn^{III}Mn^{IV}$) at 0.229 V (*vs* SCE) in $CH_3CN$, but no other reversible redox couple is observed out to 1.5 V. Consequently the higher $Mn^{IV}_2$ state is not accessible by oxidation with *tert*-butyl hydroperoxide. This is shown by the fact that **1** can be oxidized by *tert*-butyl hydroperoxide to give **2** and then **7** but that neither **2** nor **7** can be further oxidized by addition of stoichiometric amounts of *tert*-butyl hydroperoxide. Addition of a very large excess of hydroperoxide does result in the formation of a new species whose visible spectrum is characteristic of a $(salpnMn^{IV}(\mu\text{-}O))_2$ bis($\mu$-oxo) core. This complex may arise from partial decomposition of **2** at very high peroxide levels followed by oxidation of the second manganese or from a disproportionation of the $Mn^{III}Mn^{IV}$ complex to a $(salpnMn^{IV}(\mu\text{-}O))_2$ core and **1**, which can be reoxidized again to the $Mn^{III}Mn^{IV}$ oxidation state.

As pointed out, the one-electron reduction of a peroxy species must generate an oxy radical. Such reactive oxy radicals are implicated in the oxidative damage to a number of biologically important substrates including DNA, proteins, carbohydrates, and lipids.[50,51] *In vivo* iron complexes are known to initiate Fenton radical chemistry involving peroxides, which results in evolution of singlet dioxygen. Singlet oxygen evolution occurs from the reaction of excess *tert*-butyl hydroperoxide with **1**, indicative of a radical chain decomposition of the excess organic peroxide, according to a Russell-type radical scheme:[52]

$$ROOH + \mathbf{1} \rightarrow RO^{\bullet} + 2$$

$$RO^{\bullet} + ROOH \rightarrow ROH + ROO^{\bullet}$$

$$2ROO^{\bullet} \rightarrow ROOOOR \rightarrow 2RO^{\bullet} + {}^1O_2$$

$$2RO^{\bullet} \rightarrow ROOR$$

An important feature of this mechanism is the peroxy radical recombination reaction to yield, as one product, dioxygen in the singlet state. This reaction accounts for the fact that we observe *tert*-butyl alcohol as the primary product of the radical decomposition of *tert*-butyl hydroperoxide by **1**. Under dilute conditions, we also observe small amounts of the di-*tert*-butyl peroxide, ROOR, in the GC traces of the reaction mixture. Decomposition of cumyl hydroperoxide by **1** resulted in the formation of a small amount of acetophenone, characteristic of $\beta$-scission of the less stable cumyl peroxy radical. The radical source of oxygen evolution was confirmed by addition of nitrosylbenzene or cyclohexene to the reaction mixture, which resulted in essentially complete quenching of the oxygen evolution. The formation of singlet dioxygen from peroxy radical recombination is well documented[42−44] and appears to have some biological precedent as well, since the recombination of lipid peroxy radicals appears correlated with singlet dioxygen emission, as in the oxidation of linoleate catalyzed by soybean lipoxygenase[53] or from the $Mn^{2+}$ activated ribulose 1,5-bis(phosphate) oxygenase reaction.[54] This observation suggests that similar radical peroxide chemistry may be initiated by *in vivo* manganese complexes.

The primary source of *in vivo* organic oxy radicals would be lipid peroxides, which are formed by autoxidation of unsaturated fatty acids and fatty acid esters and which can be decomposed by redox-active metal complexes. Unsaturated fatty acids react by initial hydrogen atom abstraction from the allylic position,[55] followed by reaction with dissolved dioxygen to yield the lipid allyl peroxide. Since the product distribution of the cyclohexene oxidation initiated by **1** and *tert*-butyl hydroperoxide suggests the intermediacy of a 3-cyclohexenyl-1-peroxy species, it is worthwhile examining the cyclohexene oxidation observations in this context.

The oxidation of cyclohexene by the system **1** + *tert*-butyl hydroperoxide is proposed, on the basis of the observations above, to occur as in Scheme 3. The alkoxy radical $RO^{\bullet}$ is generated in the oxidation of **1**, Scheme 2, and initiates a cascade of oxidative events resulting in the formation of the oxygenated products. A hydrogen atom abstraction from the cyclohexene allyl position occurs to give the cyclohexyl radical **A**, which reacts with atmospheric oxygen to yield the cyclohexenyl hydroperoxy radical **B**, consistent with the observation of $^{18}O$ incorporation from labeled dioxygen. Chain propagation steps may include abstraction of a hydrogen from cyclohexene by **B** to give a new **A** and cyclohexene hydroperoxide, and O atom transfer from **B** to cyclohexene or to 2-cyclohexen-1-one to give cyclohexene oxide or cyclohexen-1-one oxide and the cyclohexenoxyl radical **C**.[56−60] The reaction of **B** with the olefin to form the epoxidized species in Scheme 3 is proposed since $^{18}O$-labeling studies show complete incorporation of labeled oxygen into the epoxides from atmospheric sources instead of from the *tert*-butyl hydroperoxide oxidant. A primary chain termination step may be the coupling of two cyclohexenylhydroperoxy

(47) Messinger, J.; Badger, M.; Wydrzinski, T. *Proc. Natl. Acad. Sci. U.S.A.* **1995**, *92*, 3209−3213.
(48) Silbert, L. S.; Wittnauer, L. P.; Swern, D.; Riccuitti, C. *J. Am. Chem. Soc.* **1959**, *81*, 3244.
(49) Willit, C. O.; Riccuitti, C.; Knight, H. B.; Swern, D. *Anal. Chem.* **1952**, *24*, 785.
(50) Ahmad, S. In *Oxidative Stress and Antioxidant Defenses in Biology*; Ahmad, S., Ed.; Chapman & Hall: New York, 1995.
(51) Asada, K.; Yoshikawa, T. In *Frontiers of Reactive Oxygen Species in Biology and Medicine*; Asada, K., Yoshikawa, T., Eds.; Elsevier Science: Kyoto, Japan, 1994; pp 13−70, 149−200, 431−536.
(52) Russell, G. A. *J. Am. Chem. Soc.* **1957**, *79*, 3871−3877.
(53) Kanofsky, J. R.; Axelrod, B. *J. Biol. Chem.* **1986**, *261*, 1099−1104.
(54) Mogel, S. N.; McFadden, B. A. *Biochemistry* **1990**, *29*, 8333−8337.
(55) Porter, N. A. *Acc. Chem. Res.* **1986**, *19*, 262−268.
(56) Van Sickle, D. E.; Mayo, F. R.; Gould, E. S.; Arluck, R. M. *J. Am. Chem. Soc.* **1967**, *89*, 977.
(57) de Roche, I. S. *Bull. Soc. Chim. Fr.* **1965**, 1979.
(58) Brill, W. F.; Indictor, N. *J. Org. Chem.* **1964**, *29*, 710.
(59) Brille, W. F. *J. Am. Chem. Soc.* **1963**, *85*, 141.
(60) Walling, C.; Heaton, L. *J. Am. Chem. Soc.* **1965**, *87*, 38.

**Scheme 3**

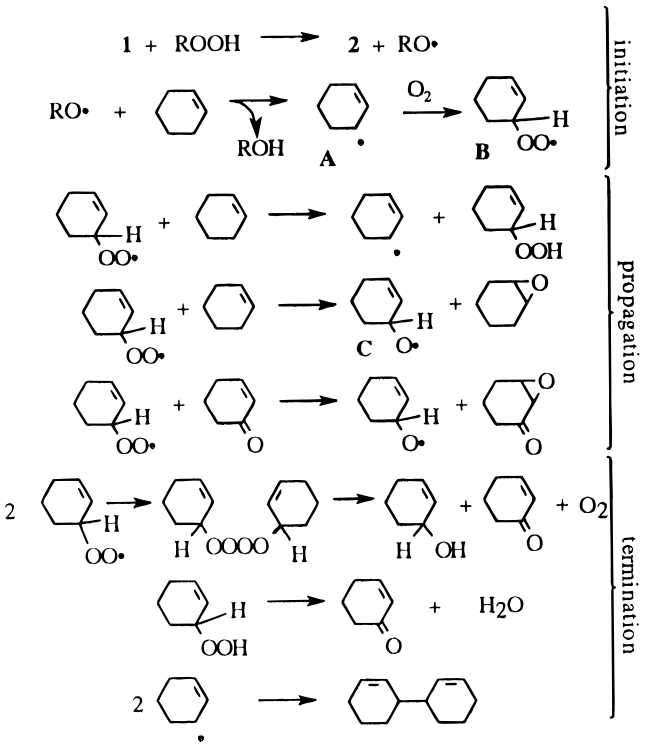


radicals, **B**, to give 2-cyclohexen-1-one, 2-cyclohexen-1-ol, and oxygen, analogous to the decomposition of tertiary alkyl tetraoxides. A second termination step will also be the decomposition of the secondary cyclohexenyl hydroperoxide to give 2-cyclohexen-1-one and water and explains why the unsaturated ketone comprises the majority of cyclohexene oxygenation products. Finally, two cyclohexenyl radicals, **A**, may combine to give bicyclohexene. All of the organic products in Scheme 3 were detected in the GC/MS analysis of the reaction mixture. The products of the oxygenation of cumene and cyclohexane can be explained by a similar chain of radical-mediated events, and the considerably lower yields in the case of cyclohexane oxidation are consistent with the stronger homolytic C−H bond strength (95 kcal/mol) compared to those of cyclohexene (85 kcal/mol) and cumene (84 kcal /mol).

As Scheme 3 suggests, the role of the metal complex **1** in this system is that of a radical initiator rather than a catalyst. This is confirmed by the fact that, in the cyclohexene oxidation experiments, dioxygen uptake and product formation continued well after **1** was completely converted into the inactive **2**. **2** itself was shown to be unreactive toward all of the organic substrates used in this study and toward the alkyl hydroperoxides.

This system illustrates the potential pitfall of interpreting the presence of small amounts of oxo-transfer products (in our case, the cyclohexene epoxides) as being indicative of the presence of high-valent metal oxo intermediates in the reaction of peroxy species with manganese complexes. There are number of characterized manganese(V) oxo complexes[17−19] and good evidence for the existence of manganese(IV) oxo intermediates in some olefin epoxidation systems.[12−16] In addition, systems which show chiral induction when catalyzed by chiral metal complexes must involve a metal complex-based oxidant.[61] However, in the case of nonheme iron systems, evidence for a ferryl oxo intermediate mechanistically required for organic functionalization is less definitive. In fact, it was recently suggested that liberated oxy radicals are the species attacking the organic substrate in certain of these systems.[3,4] This work demonstrates that this may be the case for many non-porphyrin manganese complexes as well. Therefore, it is not possible to assign the oxidation mechanism on the basis of analysis of the organic products alone, and rigorous labeling and kinetic experiments are required in order to establish the mechanism of oxidation.

**Acknowledgment.** The authors wish to thank the NIH (Grants GM39406 to V.L.P. and GM45205 to J.E.P.-H.) for financial support of this work. M.T.C. thanks the NIH (Grant GM17348) for receipt of a postdoctoral fellowship. EXAFS and XANES measurements were made at SSRL which is supported by the U.S. DOE and an NIH Research Resource Grant. We also thank Thomas A. Moore, Devens Gust, Jeffrey E. Lewis, and Manuel S. Gonzales for the singlet oxygen determinations.

**Supporting Information Available:** Tables S1 and S2, containing XANES and EXAFS fitting parameters, Figure S1, showing the equilibrium spectrum of **1** upon addition of incremental amounts of *tert*-butyl hydroperoxide, and Figures S2−S4, showing chromatograms identifying the products of the oxygenation reactions of cumene, cyclohexene, and cyclohexane (6 pages). Ordering information is given on any current masthead page.

IC951462U

(61) Zhang, W.; Loebach, J. L.; Wilson, S. R.; Jacobsen, E. N. *J. Am. Chem. Soc.* **1990**, *112*, 2801−2803.